Fermilab Library
0 1160 0034204 2

SISSA ISAS

Multiple Fragmentation Models of Centrally Condensed Molecular Cloud Cores

Leonardo Di G. Sigalotti

International School for Advanced Studies, SISSA, Strada Costiera 11,
34014 Trieste, Italy

Ref. S.I.S.S.A. 152/93/A (September 1993)

Via Beirut 2-4 - 34013 Trieste - ITALY

Abstract

The protostellar collapse of centrally condensed, rapidly rotating ($\beta \approx 0.17$) cores is investigated for initial configurations with power-law distributions ($\rho \propto r^{-n}$ with $n \geq 1$) and internal non-rotational motions. The central condensation and irrotational velocity field assumed for the initial models are consistent with the structure resulting in the early spherically symmetric collapse of an initially uniform-density, static sphere. The results imply that core models with initial differential rotation and $m = 2$ azimuthal density variations experience multiple protostar formation during the isothermal collapse through intermediate phases which first involve direct fragmentation into a stable, long-period binary and then hierarchical fragmentation of the previously formed fragments into short-period binaries. Protostellar cores of non-prolate shape may still collapse to form multiple systems by direct fragmentation if the initial conditions include also differential rotation. Initially uniformly rotating clouds undergo rapid central collapse without fragmenting to form a final central object. The observed hierarchical fragmentation is driven rotationally and results itself in a very efficient mechanism for angular momentum redistribution. It may also provide a plausible dynamical mechanism to explain the formation of close binary systems.

1 Introduction

Observations of molecular emission lines from dark clouds indicate the presence of filamentary gas condensations (e.g. Maddalena et al. 1986; de Geus, Bronfman & Thaddeus 1990) within which low-mass sub-condensations (commonly referred to as cloud cores) have been also identified (e.g. see Beichman et al. 1986). The idea that the process of star formation may take place during the evolution of these clumps comes primarily from the detection of young stellar objects associated with many surveyed cores (Beichman et al. 1986; Benson & Myers 1989; Shulz et al. 1991). This evidence has also suggested that clumps without apparent embedded sources may be in the process of forming stars. While some of these cores could be actually in advanced stages of the star formation process, perhaps containing newly formed stars with undetectable luminosities, some others could be in very early phases of the evolution thereby providing the best information about

the true initial conditions for protostellar collapse.

Inferred properties of molecular cloud cores seem to be independent of the presence or absence of young stars as suggested by the fairly well tendency of most dense cores to possess density distributions that are approximately described by power-law variations $\rho \propto r^{-2}$ (Arquilla & Goldsmith 1985; Fuller & Myers 1992) and elongated ellipsoidal shapes (Myers et al. 1991). Strong evidence for significant rotational motion in dense cores has been recently given by Goodman et al. (1993) who measured linear velocity gradients consistent with solid-body rotation in about 29 of 43 cores studied. The magnitudes of the velocity gradients were found to correspond to values of the ratio of rotational to gravitational energy (β) in the range from 2×10^{-3} to 1.4, with most cores having $\beta \sim 0.02$.

Fragmentation during the dynamical collapse phase of core evolution is the likely mechanism through which binary and multiple stellar systems are expected to form. The prevalence of rotation in molecular cloud cores is a crucial aspect of the initial conditions that enhances the possibility of fragmentation. More observational work is, however, needed to establish which condition - solid-body v.s. differential rotation - is the more appropriate for protostellar collapse. Theoretical considerations indicate that magnetic braking can efficiently redistribute angular momentum in regions with densities less than $\sim 10^6 cm^{-3}$ (Mouschovias, Paleologou & Fiedler 1985) resulting in approximate uniform rotation. The molecular cores studied by Goodman et al. (1993) have inferred mean densities $\gtrsim 10^4 cm^{-3}$ and so most of their envelope region could still have strong magnetic support. At densities higher than $\sim 10^6 cm^{-3}$, the dissipating effects of magnetic braking are expected to be reduced by rapid ambipolar diffusion (Mouschovias & Paleologou 1981; Shu 1983). In the absence of other mechanisms for angular momentum redistribution, the densest core regions should then contract with approximately conserved angular momentum, and if mass is also preserved, we may expect the core to exhibit some degree of differential rotation.

Three-dimensional (3D) collapse calculations with uniformly rotating initial conditions indicate that rapidly rotating ($\beta \gtrsim 0.16$) core models with $m = 2$ density variations, may evolve into multiple protostellar systems during their isothermal infall phase as a result of rotation-driven fragmentation

(Boss 1991; Klapp, Sigalotti & de Felice 1993). Further calculations by Boss (1993) have shown that even for initial low values of $\beta(\lesssim 0.0024)$, prolate cores with initial solid-body rotation may collapse isothermally to intermediate cylindrical forms before fragmenting into binary and eventually higher-order (hierarchical) systems. Uniform rotation, however, may result in a less favourable condition for binary and multiple fragmentation in dense cores of non-prolate shape. Recent calculations of moderately centrally condensed cores of small size ($\lesssim 0.025pc$) along with implicitly assumed $m = 4$ density perturbations, support this conclusion (Sigalotti & Klapp 1993). In spite of the relatively initial high rotation ($\beta = 0.20$) for these models, the central core regions collapsed to form only single fragments by the end of the isothermal regime even for initially low values of the ratio of the thermal to gravitational energy $\alpha(= 0.05)$.

While the above results may apply to low-mass star formation from mild central condensations, only a few model calculations have been made starting with much steeper radial density gradients ($\rho \propto r^{-n}$, with $n \geq 1$) and higher degrees of central condensation (Myhill & Kaula 1992; Sigalotti 1993). In particular, Myhill & Kaula (1992) compare the effects of including uniform and differential rotation in the initial conditions for models with $\beta \approx 0.17$ and density distributions varying as r^{-1} and r^{-2}. They found that all of the differentially rotating cores fragmented into well-defined binaries while the uniformly rotating models collapsed dynamically to produce a dense central object. Multiple protostellar formation, however, may result in differentially rotating configurations if the initial conditions include internal irrotational motions. This possibility has been considered by Sigalotti (1993) who found that a small radially-directed velocity field if initially present in the structure of a dense core can induce sizeable non-axisymmetry which then amplifies during collapse resulting in multiple (hierarchical) fragmentation. Following this direction, this paper describes the details of three new high-resolution, collapse model calculations of centrally condensed cores with an initial prescribed radial velocity field ($v_r \neq 0$). The models are chosen to explore the effects of (i) including uniform v.s. differential rotation, (ii) varying the amount of thermal energy and (iii) replacing the initially $m = 2$ density variation, used to mimic the elongated ellipsoidal shapes of real molecular cloud cores (Myers et al. 1991), with a random noise variation of the density in the

azimuthal coordinate. This latter form of the density perturbation would be more representative of cloud cores with oblate-like shapes.

The models with initial differential rotation and $m = 2$ density variations experienced multiple protostellar formation through intermediate phases first involving direct fragmentation into a stable, long-period binary and then successive hierarchical fragmentation of the previously formed components into short-period binaries. Multiple formation is also observed to occur when the $m = 2$ density perturbation is replaced by a random noise variation. In this case, the multiple protostellar system formed by direct fragmentation resulting from the gravitational growth of non-axisymmetric perturbations during collapse. Only when the initial conditions include uniform rotation is fragmentation avoided. In this case, non-homologous central collapse leads to the rapid formation of of a central ellipsoidal core. Hierarchical fragmentation results in a very efficient mechanism for angular momentum redistribution during the early dynamical collapse of dense cores.

2 Protostellar Collapse Models

The initial conditions used for the protostellar collapse calculations are summarized in Table 1. Models I and II have been previously described by Sigalotti (1993) and are included here to facilitate comparisons with case III which differs from the former models in the form of the initial rotation pattern. Furthermore, models II and IV define a sequence of collapse calculations with increasing amount of the thermal energy (values of α) while cases IV and V have similar initial conditions except for the azimuthal density variation assumed. The entries in Table 1, starting from the second column, give respectively, the total core mass in units of the solar mass, the average initial density, the initial values of the density and angular velocity at approximately half the radius of the protostellar core, the specific (spin) angular momentum, the total cloud radius, the initial ratio of the thermal to the gravitational energy, the initial rotation pattern and the type of the density perturbation assumed. The values of $\tilde{\omega}$ have been chosen so that the initial ratio of the rotational to gravitational energy $\beta \approx 0.17$ for all cases. Thus the models apply to low-mass star formation from rapidly rotating protostellar cores.

The initial central condensation of the 3D core models is consistent with the density profile resulting at some early stage in the spherically symmetric (1D) collapse of an initially uniform-density, static sphere. Two distinct 1D models were considered. One model corresponds to an initial spherical cloud of density $\rho_0 = 6.102 \times 10^{-20} gcm^{-3}$ and mass $M = 6M_\odot$ (Model A) and the other one to a sphere of initial density $\rho_0 = 1.430 \times 10^{-19} gcm^{-3}$ and mass $M = 9M_\odot$ (Model B). Assuming pure molecular hydrogen and a constant temperature $T = 10K$, models A and B result in Jeans-unstable configurations with $\alpha = 0.47$ and 0.27, respectively. For both cases, the time evolution was calculated with $n_r = 45$ moving radial grid-points using the 1D version of a new finite-difference, hydrodynamic code which is second-order accurate in space and first-order accurate for the temporal discretization (Sigalotti, in preparation). The resulting density profiles are shown in Fig. 1 at $0.912t_{ff}$, where $t_{ff} = \sqrt{3\pi/32G\rho_0}$, for model A and at $0.868t_{ff}$ for case B when the central density, ρ_c, is about 200 times higher than the cloud boundary density, ρ_b. Note that cloud model A results in a shorter central density plateau and in a less steep gradient ($\rho \propto r^{-1.692}$) for the envelope region than model B which has $\rho \propto r^{-2.695}$. This difference in slopes is a consequence of the fact that isothermally collapsing clouds with lower associated thermal energy tend to develop larger intermediate infall velocities thereby resulting in more gas depletion in the outermost regions (Sigalotti 1993). By the times of Fig. 1, model B with $\alpha = 0.27$ reaches a maximum radial velocity $v_r \approx 3.23c_s$, where c_s denotes the sound speed, in the envelope regions against $v_r \approx 2.16c_s$ for model A initially with a higher value of α. For comparison, Fig. 1 also shows the density profile resulting from a further 1D model calculation initially with $\alpha = 0.06$ (Model C). By $0.640t_{ff}$ when $\rho_c/\rho_b \approx 200$, the collapse results in a much larger central density plateau and in a much steeper density gradient ($\rho \propto r^{-8.177}$) for the cloud envelope with maximum infall velocities $\approx 4.89c_s$ in this region.

The numerical profile resulting from the early evolution of model B is used to define the initial central condensation of models I-III while that obtained for model A is used for cases IV and V. In order to mimic the observed elongated shapes of molecular cloud cores, an $m = 2$ density variation

is added to the spherically symmetric radial profiles so that

$$\rho(r,\theta,\phi) = \rho^{1D}(r)\,(1 + 0.3\cos 2\phi) \quad , \tag{1}$$

for all models with the exception of case V which has initially

$$\rho(r,\theta,\phi) = \rho^{1D}(r)\,[1 + 0.3 \cdot RAN(\phi)] \quad , \tag{2}$$

where $RAN(\phi)$ is a random number in the interval (0,1). This form would be more representative of centrally condensed cores beginning to collapse with an oblate-like shape.

Only model I is allowed to evolve from a perfectly static configuration as most previous protostellar collapse calculations. The rest of the models begins the collapse with an initial radially-directed velocity field given by

$$v_r(r,\theta,\phi) = v_r^{1D}\,[1 + 0.1 \cdot RAN(\phi)] \quad , \tag{3}$$

where v_r^{1D} is the spherically symmetric (1D) velocity field of models A and B at the times corresponding to the profiles of Fig. 1 multiplied by a constant factor $f = 0.1$ for consistency with observations which suggest that most dense cores are likely to be in a state of critical near-equilibrium, and $RAN(\phi)$ is a random number in the interval (-1,+1). The initial conditions are finally specified by defining the differential angular velocity profile

$$\omega(r,\theta,\phi) = \tilde{\omega}\left\{\frac{\rho(r,\theta,\phi)}{\tilde{\rho}}\right\}^{2/3}[1 + b \cdot RAN(\phi)] \quad , \tag{4}$$

where a random number in the interval (0,1) is also added to introduce a noisy dependence of ω with the ϕ-coordinate. Only model III starts collapsing with uniform rotation and so for this case the value of $\tilde{\omega}$ in Table 1 corresponds to the initial constant angular velocity ω_0. The assumption of differential rotation is consistent with the central core regions (see Fig. 1) having molecular hydrogen densities $\gtrsim 5.0 \times 10^5 cm^{-3}$. Theoretical studies indicate that above these values rapid ambipolar diffusion is expected to lessen the effects of magnetic braking causing the densest core regions to contract with approximately conserved angular momentum (Mouschovias, Paleologou & Fiedler 1985).

The calculations are made using a spatially second-order code (Sigalotti, in preparation) with a grid resolution consisting of $n_r = 45$ non-uniformly distributed radial points, $n_\theta = 33$ fairly equidistant points along the θ-direction (with no reflection symmetry about the equatorial plane $\theta = \pi/2$) and $n_\phi = 80$ uniformly spaced points in the azimuthal coordinate covering the full 2π radians, resulting in a total number of $1 + n_r(2 + n_\theta n_\phi) = 118891$ cells. The free-fall time scale used to measure the time evolution is here defined as $t_{ff} = \sqrt{3\pi/32G\rho_{av}}$, where ρ_{av} refers to the initial average density listed in Table 1. The same definition of t_{ff} was also employed by Myhill & Kaula (1992) for collapse calculations with power-law density distributions.

Table 2 lists the relevant properties of the resulting configurations. The columns in this table, starting from the second, give respectively, the time (in free-fall time units) at which the integral properties were evaluated, the mass of the fragments in terms of the total core mass M, their specific (spin) angular momentum relative to the value of the original cloud, the approximate fragment mean diameters and half-distances of binary separation in terms of the initial core radius R_0, the critical separation for binary survival (or merging) using Boss (1986) criterion and the estimated values of α and β for the fragments. For asymmetric binaries, Boss' criterion for binary survival can be written as

$$\left(\frac{d}{R_0}\right) > \left(\frac{d}{R_0}\right)_{cr} = 0.06786 \cdot \left(\frac{M_1 + M_2}{2M}\right)^{1/3} , \tag{5}$$

where M_1 and M_2 denote the masses of the binary components, M refers to the mass of the placental cloud from which the binary formed and d is one-half of the binary separation distance.

The details of the time evolution underwent by models I and II are fully described by Sigalotti (1993). Case I, initially with $v_r = 0$, formed a stable binary system as a result of the differentially rotating initial conditions in good agreement with Myhill & Kaula (1992) results. Model II with identical initial conditions to case I, except for the magnitude of the radial velocity field ($v_r \neq 0$), produced a multiple $m = 6$ protostellar core which resulted from the successive hierarchical fragmentation of a previously formed, long-period binary. The final configuration obtained for this model calculation is shown in Fig. 2 which displays equatorial density contours for the inner cloud

regions at $0.756t_{ff}$. A linear perturbation analysis demonstrated that the enhanced fragmentation observed for this model may be attributed to the presence of internal irrotational motions combined with the differential rotation in the initial structure of the cloud (see Sigalotti 1993). In a pressure-supported configuration, significant irrotational motion can always generate oscillations of finite amplitude in the rotational field component which then may rapidly amplify in zones of high density. The amount of sizeable non-axisymmetry is further increased by the initial presence of differential rotation and by the radial infall velocity components generated by the cloud's self-gravitation which also involve oscillations in v_ϕ.

The effects of including uniform rotation in the initial conditions are shown in the sequence of equatorial density contours of Fig. 3 for the time evolution of model III. Because of the initial $m = 2$ density perturbation, the central core regions become rapidly unstable to binary fragmentation (Fig. 3a). Soon after $0.30t_{ff}$, the $m = 2$ mode decays into a bar-like pattern as a result of the strong central collapse (Fig. 3b at $0.325t_{ff}$). This is one crucial difference with the evolution of model II, where the central regions initially at a higher rotational rate than the rest of the cloud retarded the central infall allowing the $m = 2$ instability to grow before the occurrence of high central densities. One further aspect is the shortening of the time-scale for collapse as evidenced in Fig.3c at $0.359t_{ff}$ when $\rho_{max} \sim 16191\rho_{av}$. At this time, an $m = 2$ density structure is, however, still present in the innermost central bar which then merge to form a central ellipsoidal core by $0.365t_{ff}$ (Fig. 3d) when $\rho_{max} \sim 75254\rho_{av}$. The central core appears to be highly flattened about the equatorial plane and contains nearly 13% of the total cloud mass. It is not centrally condensed but possesses rather a clumpy structure as shown in Fig. 4 for the same plot of Fig. 3d but now including only the first nine cells in radius. The contour lines for this plot were generated using a spline interpolation scheme to better resolve the central regions. The linearly arranged small-scale condensations in Fig. 4 have masses $< 1.0 \times 10^{-3} M_\odot$ by $0.365t_{ff}$ and so they cannot represent true protostellar fragments. Furthermore, the clumps are close enough to one another that they could plausibly merge rather than survive as individual entities in the later evolution. The results of this model calculation, however, are qualitatively in agreement with Myhill & Kaula (1992) predictions that

initially uniformly rotating clouds with power-law distributions and implict $m = 2$ perturbations, avoid large-scale fragmentation collapsing all the way to produce a central condensation. The inclusion of an initial radially-directed velocity field, however, resulted in rapid central collapse and in the formation of a narrow central ellipsoidal core with a clumpy structure. As predicted by the linear perturbation analysis of Sigalotti (1993), this fragmentary structure arises in the regions of maximum cloud density due to the rapid amplification of rotational oscillations induced by the irrotational field components.

The sequence of Fig. 5 illustrates the time evolution for model IV initially with differential rotation and increased thermal energy ($\alpha = 0.27$). During the first free-fall time, the intermediate collapse forms for this model were almost similar to those experienced by case II. The central regions become rapidly unstable to binary fragmentation (Fig. 5a) and as a result of the higher thermal pressure, the binary formation process occurs at lower density contrasts (Fig. 5b) and on a larger time-scale (Fig. 5c) as compared with model II. Thereafter the evolution proceeds with the forming binary collapsing to even higher densities as shown in Fig. 5d at $1.019t_{ff}$. By this time, a long tail had also formed ahead of each binary component which then begins to condense at one end. Slightly later, the binary components sub-fragment (Fig. 5e at $1.059t_{ff}$) into asymmetric, short-period binaries as is evident in Fig.5f at $1.139t_{ff}$ when the calculation is terminated. Note that by this time, the weak tail condensations have also experienced hierarchical fragmentation into a new couple of binary systems leading to an $m = 8$ protostellar core. The weak fragments have densities $\lesssim 4.20 \times 10^{-16} gcm^{-3}$ and are just collapsing as separate entities. Table 2 summarizes the integral properties of the resulting configuration. Nearly 30% of the total cloud mass is contained by the dominant, long-period binary while only 5% is in form of newly formed condensations. The densest fragments have so low values of α that they could experience further fragmentation later in the evolution. Since the $m = 8$ protostellar core (Fig. 5e) may be interpreted as a system of four protostellar binaries, Boss (1986) criterion for binary survival (eq. 5) can be applied in principle to make a rough prediction for stability. As shown in Table 2, the newly formed binaries are found to be stable according to this criterion while the systems consisting of a dominant and weak fragment

resulted to be unstable. The dominant components have much higher densities and larger sizes than the weak companions and so the latter could be tidally disrupted or even induced to merge as a result of loss of their orbital angular momentum due to the strong tidal attraction exerted by the denser components. The prediction of orbital stability for the newly formed binary has been made ignoring the influence of the other nearby fragments and so we cannot definitely conclude that they will survive to become stars. Accretion of high angular momentum gas, orbital decay through gravitational torques from the cloud envelope and nearby condensations, gas drag and rapid central rotation are effects that may compromise the stability of the multiple system. The time-scales for collapse, however, are smaller than those required for orbital decay (Boss 1984), and hence we may expect some of the hierarchical binaries in model IV to condense before undergoing merging.

Model V was given a random noise perturbation and so it could better represent a centrally condensed core of oblate shape. This model collapsed to form a circular ring by $0.551t_{ff}$ which fragmented while growing in size. The final configuration obtained is shown in Fig. 6 at $1.066t_{ff}$ when three dominant fragments had formed. At this time, the fragmenting ring is still nearly circular with the regions between the larger fragments having also split up into small condensations. These regions have, however, accumulated sufficient mass to allow some of these clumps to accrete mass during the further evolution perhaps leading to an $m > 3$ protostellar core. In this case, fragmentation is not driven rotationally as in the previous models but rather induced by the gravitational growth of non-axisymmetric perturbations during ring collapse.

From Table 2 we see that the more massive fragments which formed by direct gravitational amplification of the initial perturbation have their spin angular momentum reduced by factors ranging from 5.38 to 19.61 with respect to the initial cloud value. The short-period binaries in models II and IV resulting from hierarchical fragmentation have larger reduction factors ranging from 23.26 to 66.66. This clearly shows that hierarchical fragmentation during a single collapse phase may result in a very efficient mechanism for angular momentum redistribution. A further important aspect of the results is that the binary separation distances of the hierarchical systems are factors of 3 to 5 shorter than the separation distance of the long-period binaries arising by

direct fragmentation. Thus we may expect that further sub-fragmentation before the formation of the first quasi-equilibrium core may provide a plausible dynamical mechanism to explain the formation of close binary systems.

3 Conclusions

Numerical solutions have been presented for the isothermal collapse and fragmentation of strongly centrally condensed, rapidly rotating ($\beta \approx 0.17$) protostellar core models with initial conditions corresponding as close as possible to inferred properties of low-mass, molecular cloud cores. The calculations were performed using a new second-order accurate hydrodynamic code with high resolution. The effects of including small non-rotational motions in the initial conditions were assessed for cloud models having uniform and differential rotation, varied thermal energy and azimuthal density perturbations appropriate for prolate- and oblate-like shapes. The central condensation and radial velocity field assumed for the initial models are consistent with the structure resulting in the early collapse of a spherically symmetric (1D) cloud. The relevant conclusions which arise from this investigation are summarized in the following points:

1. Rapidly rotating ($\beta \approx 0.17$) protostellar cores with power-law density distributions r^{-n} and high degrees of central condensation may result in multiple protostar formation during the first dynamical collapse only if the initial conditions include differential rotation and internal irrotational motions. Contrarily, uniform rotation is seen to be a less favourable condition for fragmentation in agreement with Myhill & Kaula (1992) results.

2. Differentially rotating cores with initial $m = 2$ density perturbations first undergo direct fragmentation into a stable, long-period binary. The multiple protostellar system arises as the previously formed binary components fragment hierarchically into short-period binaries which in turn may sub-fragment into new binary systems. The hierarchical binaries form isothermally by rotation-driven fragmentation at central core densities well below the typical values needed for non-isothermal collapse.

3. Differentially rotating cores of non-prolate shape may also form multiple systems during

the isothermal collapse by direct fragmentation as a consequence of the gravitational growth of non-axisymmetric background perturbations.

4. By the end of the calculations, the denser and larger fragments which formed by direct fragmentation have so low values of $\alpha(< 0.1)$ that they could fragment in the further evolution. These condensations contain more than 30% of the total cloud mass and have specific (spin) angular momentum reduced by factors of 5.38 to 19.61 with respect to the original cloud value.

5. The hierarchically formed fragments have masses ranging from 0.012 to $0.027 M_{\odot}$ which are appropriate for newly formed protostellar condensations. They are in a phase of early isothermal collapse with values of α of 0.194 to 0.702 and β of 0.154 to 0.892, and have spin angular momentum reduced by factors of 23.26 to 66.66 with respect to the original cloud. Thus hierarchical fragmentation results in a very efficient mechanism for angular momentum redistribution.

6. Finally, the separation distances of the hierarchically formed binaries are factors of 3 to 5 shorter than those of the long-period binaries resulting by direct fragmentation. This provides a plausible dynamical mechanism to explain the formation of close binary systems.

Acknowledgments

The calculations of this paper were performed on the CRAY YMP-18 supercomputer of the Università degli Studi di Trieste. This work was supported in part by the Ministero Italiano dell'Università e della Ricerca Scientifica e Tecnologica.

References

Arquilla R. & Goldsmith P. F., 1985, ApJ **297**, 436.

Beichman C. A., Myers P. C., Emerson J. P., Harris S., Mathieu R., Benson P. J. & Jennings R. E., 1986, ApJ **307**, 337.

Benson P. J. & Myers, P. C., 1989, ApJS **71**, 89.

Boss A. P., 1984, MNRAS **209**, 534.

Boss A. P., 1986, ApJS **62**, 519.

Boss A. P., 1991, Nat **351**, 298.

Boss A. P., 1993, ApJ **410**, 157.

de Geus E. J., Bronfman L. & Thaddeus P., 1990, A&A **231**, 137.

Fuller G. A. & Myers P. C., 1992, ApJ **384**, 523.

Goodman A. A., Benson P. J., Fuller G. A. & Myers P. C., 1993, ApJ **406**, 528.

Klapp J., Sigalotti L. Di G. & de Felice F., 1993, A&A **273**, 175.

Maddalena R. J., Morris M., Moscowitz J. & Thaddeus P., 1986, ApJ **303**, 375.

Mouschovias T. Ch. & Paleologou E. V., 1981, ApJ **246**, 48.

Mouschovias T. Ch., Paleologou E. V. & Fiedler R. A., 1985, ApJ **291**, 772.

Myers P. C., Fuller G. A., Goodman A. A. & Benson P. J., 1991, ApJ **376**, 561.

Myhill E. A. & Kaula W. M., 1992, ApJ **386**, 578.

Shu F. H., 1983, ApJ **273**, 202.

Shulz A., Güsten R., Zylka R. & Serabyn E., 1991, A&A **246**, 570.

Sigalotti L. Di G., 1993, A&A in press.

Sigalotti L. Di G. & Klapp J., 1993, MNRAS submitted.

FIGURE CAPTIONS

Fig. 1: Density profiles resulting from the spherically symmetric (1D) isothermal collapse of an initially uniform-density, static sphere with (A) $M = 6M_\odot$ and $\alpha = 0.47$ at $0.912t_{ff}$, (B) $M = 9M_\odot$ and $\alpha = 0.27$ at $0.868t_{ff}$, (C) $M = 16M_\odot$ and $\alpha = 0.06$ at $0.640t_{ff}$. Also shown is the slope of the cloud envelope region for each model. The profiles A and B are used to define the initial central condensation of the 3D protostellar core models.

Fig. 2: Equatorial density contour plot showing the final configuration obtained for model II at $0.756t_{ff}$ when $\rho_{max} = 43321\rho_{av}$. The numbers on the box sides are given $\times 10^{16} cm$. The region contoured includes 16 radial cells from the centre. Minus signs denote density minima.

Fig. 3: Equatorial density contour plots for model III: (a) at $0.208t_{ff}$, $\rho_{max} = 22\rho_{av}$; (b) at $0.325t_{ff}$, $\rho_{max} = 313\rho_{av}$; (c) at $0.359t_{ff}$, $\rho_{max} = 16191\rho_{av}$; (d) at $0.365t_{ff}$, $\rho_{max} = 75254\rho_{av}$. The numbers on the box sides are given $\times 10^{16} cm$. The region contoured includes 8 radial cells from the centre for (a), 10 for (b) and 16 for (c) and (d). Counterclockwise rotation is assumed.

Fig. 4: Same contour plot of Fig. 3d for model III at $0.365t_{ff}$ but now including only 9 radial cells from the centre. Minus signs denote density minima.

Fig. 5: Equatorial density contour plots for model IV: (a) at $0.214t_{ff}$, $\rho_{max} = 22\rho_{av}$; (b) at $0.612t_{ff}$, $\rho_{max} = 140\rho_{av}$; (c) at $0.820t_{ff}$, $\rho_{max} = 949\rho_{av}$; (d) at $1.019t_{ff}$, $\rho_{max} = 12958\rho_{av}$; (e) at $1.059t_{ff}$,

$\rho_{max} = 18878\rho_{av}$; (f) at $1.139t_{ff}$, $\rho_{max} = 29706\rho_{av}$. The numbers on the box sides are given $\times 10^{16} cm$. The region contoured includes 22 radial cells from the centre for (a), 19 for (b) and (c) and 15 for (d)-(f). Counterclockwise rotation is assumed. Minus signs denote density minima.

Fig. 6: Equatorial density contour plot showing the final configuration obtained for model V at $1.066t_{ff}$ when $\rho_{max} = 18431\rho_{av}$. The numbers on the box sides are given $\times 10^{16} cm$. The region contoured includes 15 radial cells from the centre. Minus signs denote density minima.

TABLE 1

Initial Conditions for 3D Protostellar Core Models

Model	$M/M_\odot$	ρ_{av} (gcm^{-3})	$\tilde{\rho}$ (gcm^{-3})	$\tilde{\omega}$ (s^{-1})	J/M (cm^2s^{-1})	R_0 (cm)	α	Rot.	Pert.
I[a]	9.0	2.25(-19)	1.10(-18)	1.93(-13)	2.95(21)	3.10(17)	0.15	Diff.	$m = 2$
II	9.0	2.25(-19)	1.10(-18)	1.93(-13)	2.95(21)	3.10(17)	0.15	Diff.	$m = 2$
III[b]	9.0	2.25(-19)	1.10(-18)	3.14(-13)	4.52(21)	3.10(17)	0.15	Unif.	$m = 2$
IV	6.0	1.16(-19)	7.98(-19)	1.59(-13)	2.62(21)	3.60(17)	0.27	Diff.	$m = 2$
V	6.0	1.16(-19)	7.98(-19)	1.69(-13)	2.80(21)	3.60(17)	0.24	Diff.	Noise

[a]This model has initially $v_r = 0$.
[b]Solid-body rotation is assumed for this model and so $\tilde{\omega} = \omega_0$.

TABLE 2

Fragment properties for protostellar core models[a]

Model	t/t_{ff}	M_f/M_i	$\frac{(J/M)_{spin,f}}{Reduction}$	D_f/R_0	d/R_0	$(d/R_0)_{cr}$	α_f	β_f
I	1.572	0.219	0.186	0.0521	0.171	0.040	0.029	0.332
		0.202	0.153	0.0460			0.028	0.277
II	0.756	0.140	0.090	0.0292	0.085	0.035	0.026	0.214
		0.130	0.083	0.0263			0.025	0.217
		0.007	0.027	0.0145	0.031	0.014	0.271	0.465
		0.010	0.043	0.0181			0.225	0.600
		0.004	0.035	0.0147	0.020	0.010	0.443	0.528
		0.003	0.023	0.0136			0.573	0.454
III[b]	0.365	0.126		0.006			0.037	0.281
IV	1.138	0.164	0.093	0.0317	0.029	0.030	0.042	0.203
		0.002	0.020	0.0119			0.702	0.829
		0.144	0.076	0.0291	0.025	0.029	0.044	0.154
		0.006	0.031	0.0193			0.566	0.583
		0.004	0.017	0.0188	0.018	0.014	0.649	0.673
		0.014	0.056	0.0110			0.316	0.598
		0.005	0.015	0.0174	0.019	0.016	0.466	0.428
		0.021	0.044	0.0099			0.194	0.540
V	1.066	0.079	0.051	0.0192			0.057	0.191
		0.107	0.089	0.0267			0.058	0.314
		0.054	0.068	0.0212			0.092	0.463

[a]The numbers of rows characterizing each model entry varies according to the number of fragments produced.
[b]This model collapsed to form a central ellipsoidal core.

FIG. 1

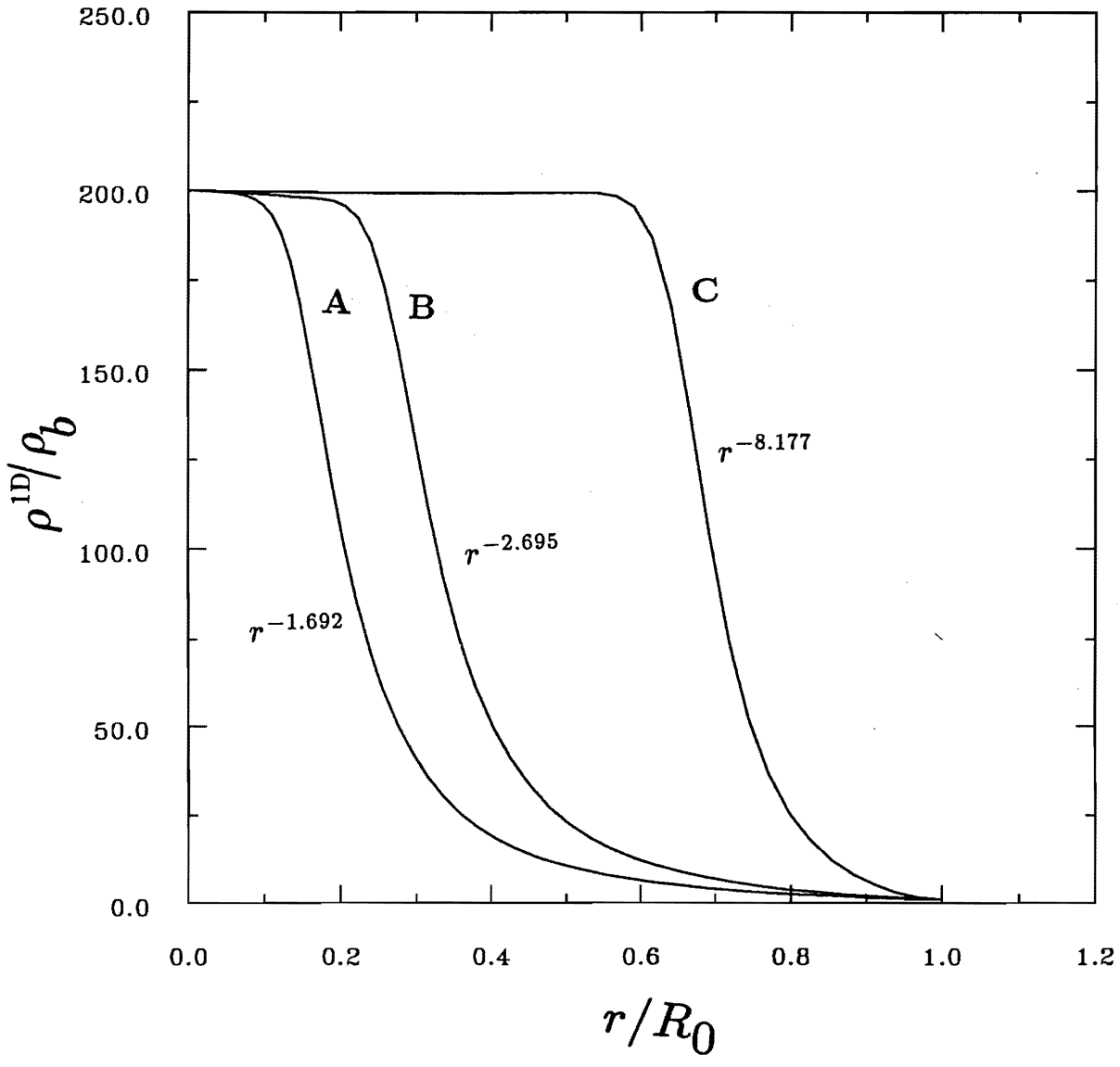
250.0
200.0
150.0
100.0
50.0
0.0
0.0
0.2
0.4
0.6
0.8
1.0
1.2
ρ^{1D}/ρ_b
r/R_0
A
B
C
$r^{-1.692}$
$r^{-2.695}$
$r^{-8.177}$

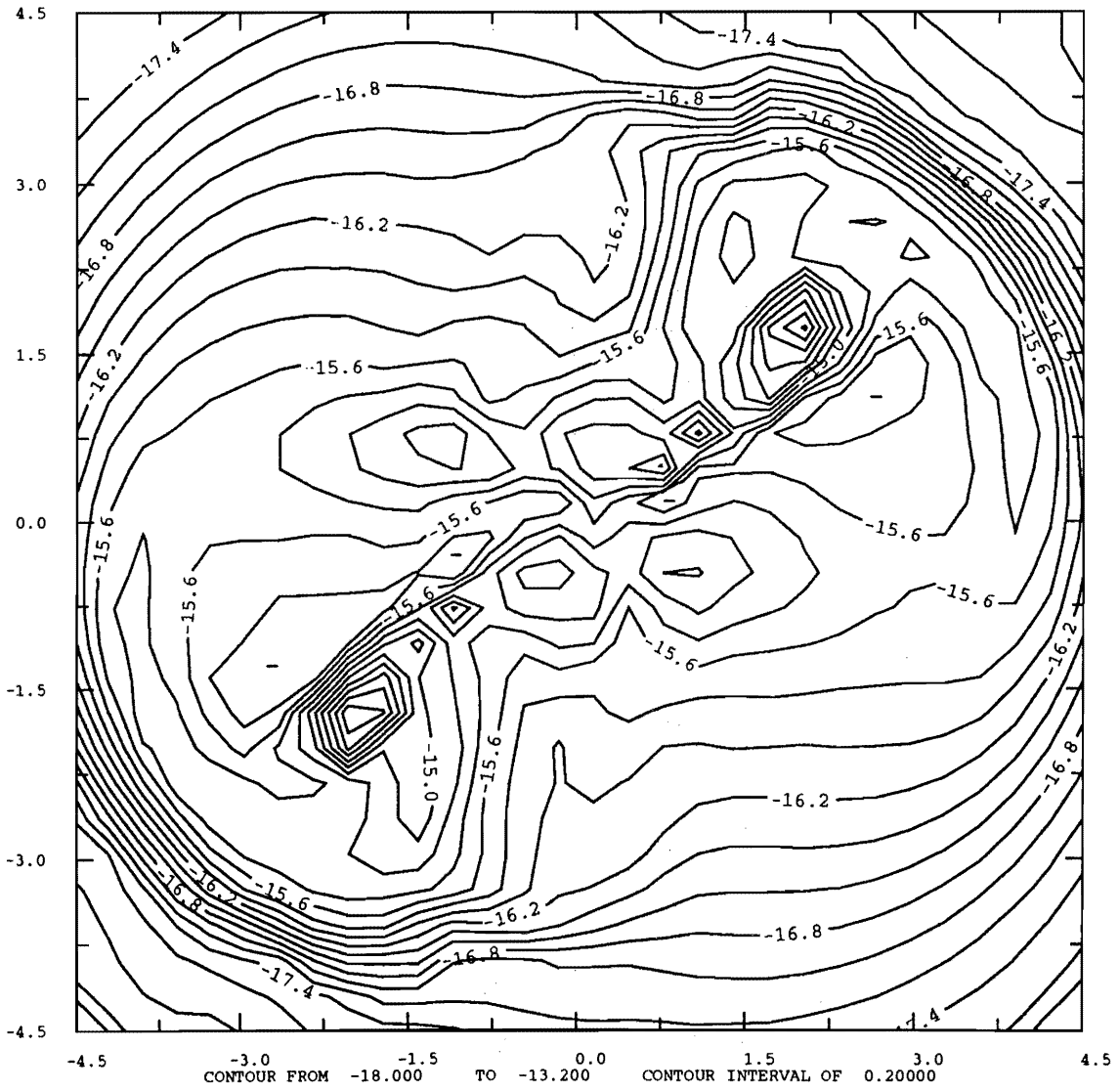
4.5
3.0
1.5
0.0
-1.5
-3.0
-4.5
-4.5
-3.0
-1.5
0.0
1.5
3.0
4.5
CONTOUR FROM -18.000 TO -13.200 CONTOUR INTERVAL OF 0.20000
-17.4
-16.8
-16.2
-15.6
-15.0

FIG. 2

(a)

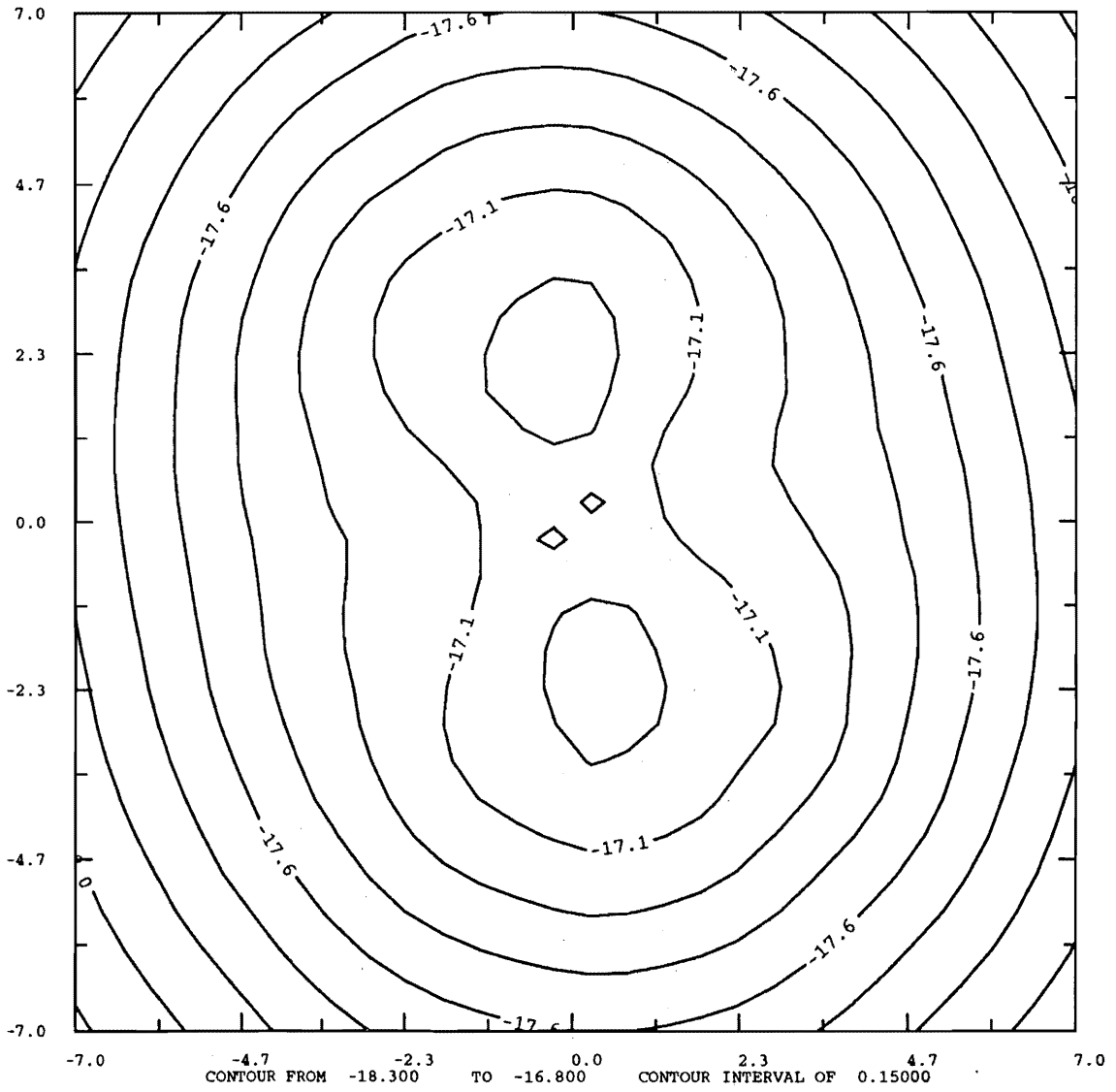
7.0
4.7
2.3
0.0
-2.3
-4.7
-7.0
-7.0
-4.7
-2.3
0.0
2.3
4.7
7.0
-17.6
-17.1
CONTOUR FROM -18.300 TO -16.800 CONTOUR INTERVAL OF 0.15000

FIG. 3a

(b)

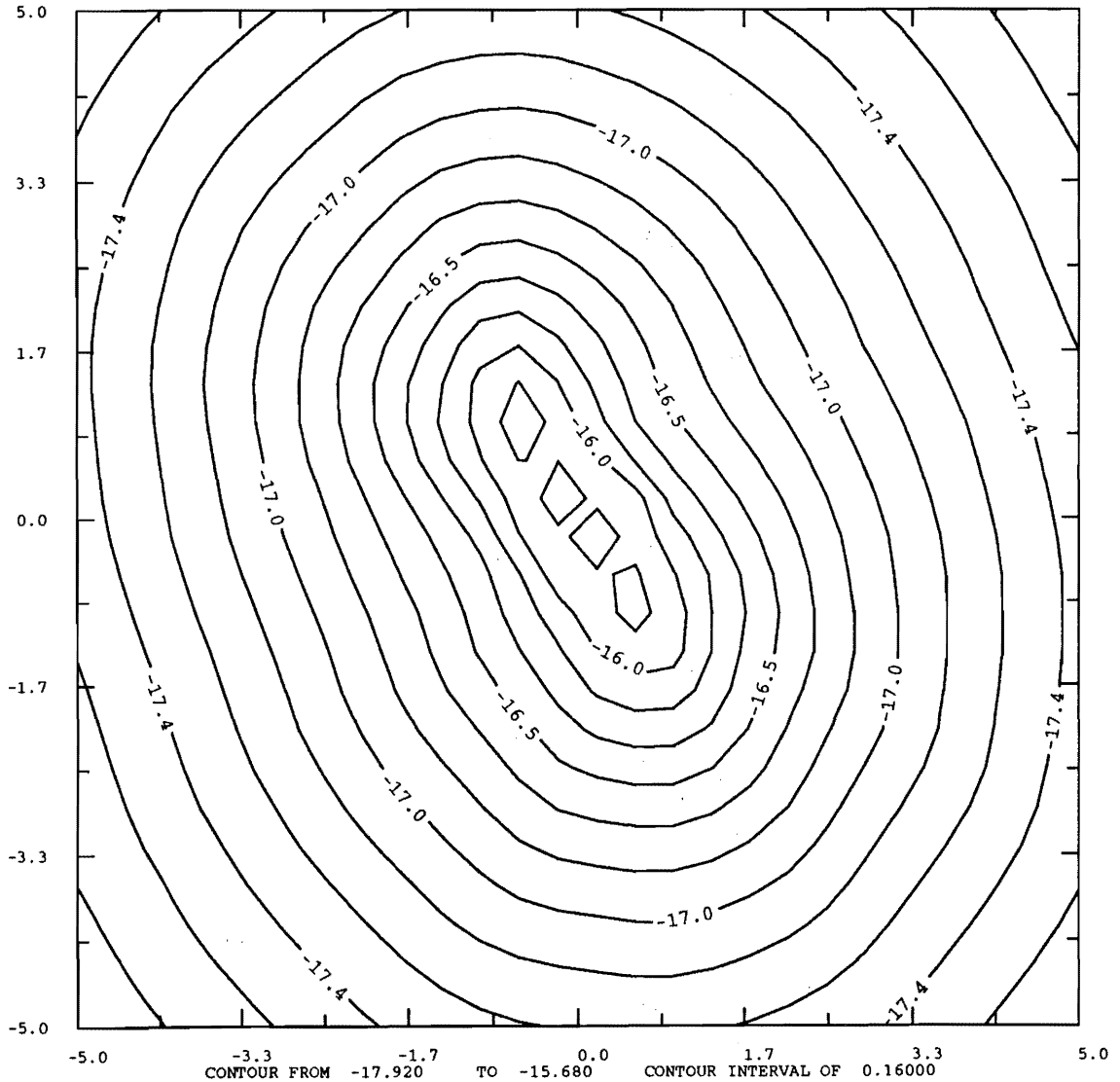
5.0
3.3
1.7
0.0
-1.7
-3.3
-5.0
-5.0
-3.3
-1.7
0.0
1.7
3.3
5.0
-17.4
-17.0
-16.5
-16.0
CONTOUR FROM -17.920 TO -15.680 CONTOUR INTERVAL OF 0.16000

FIG. 3b

(c)

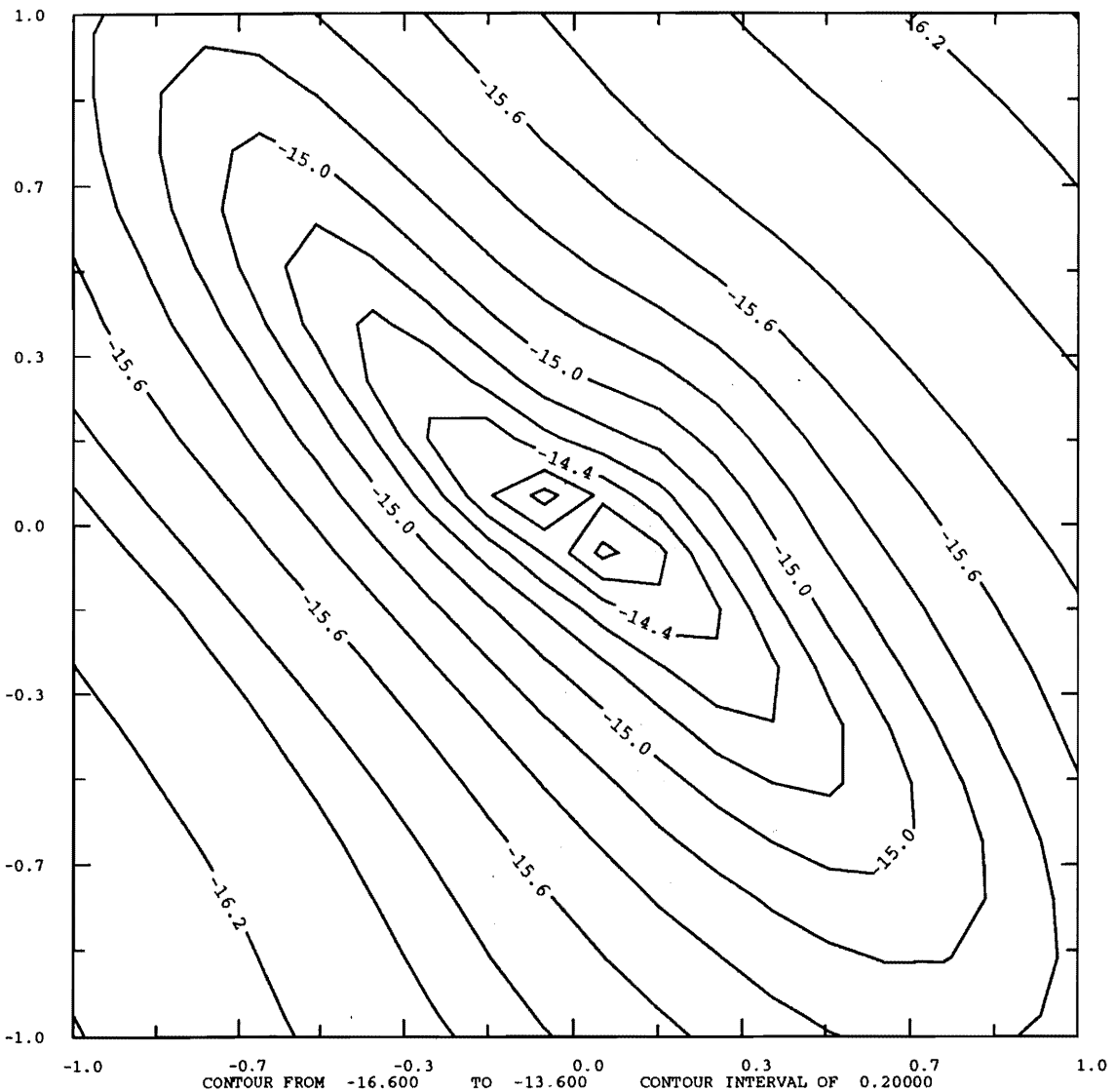
1.0
0.7
0.3
0.0
-0.3
-0.7
-1.0
-1.0
-0.7
-0.3
0.0
0.3
0.7
1.0
-16.2
-15.6
-15.0
-14.4
CONTOUR FROM -16.600 TO -13.600 CONTOUR INTERVAL OF 0.20000

FIG. 3c

(d)

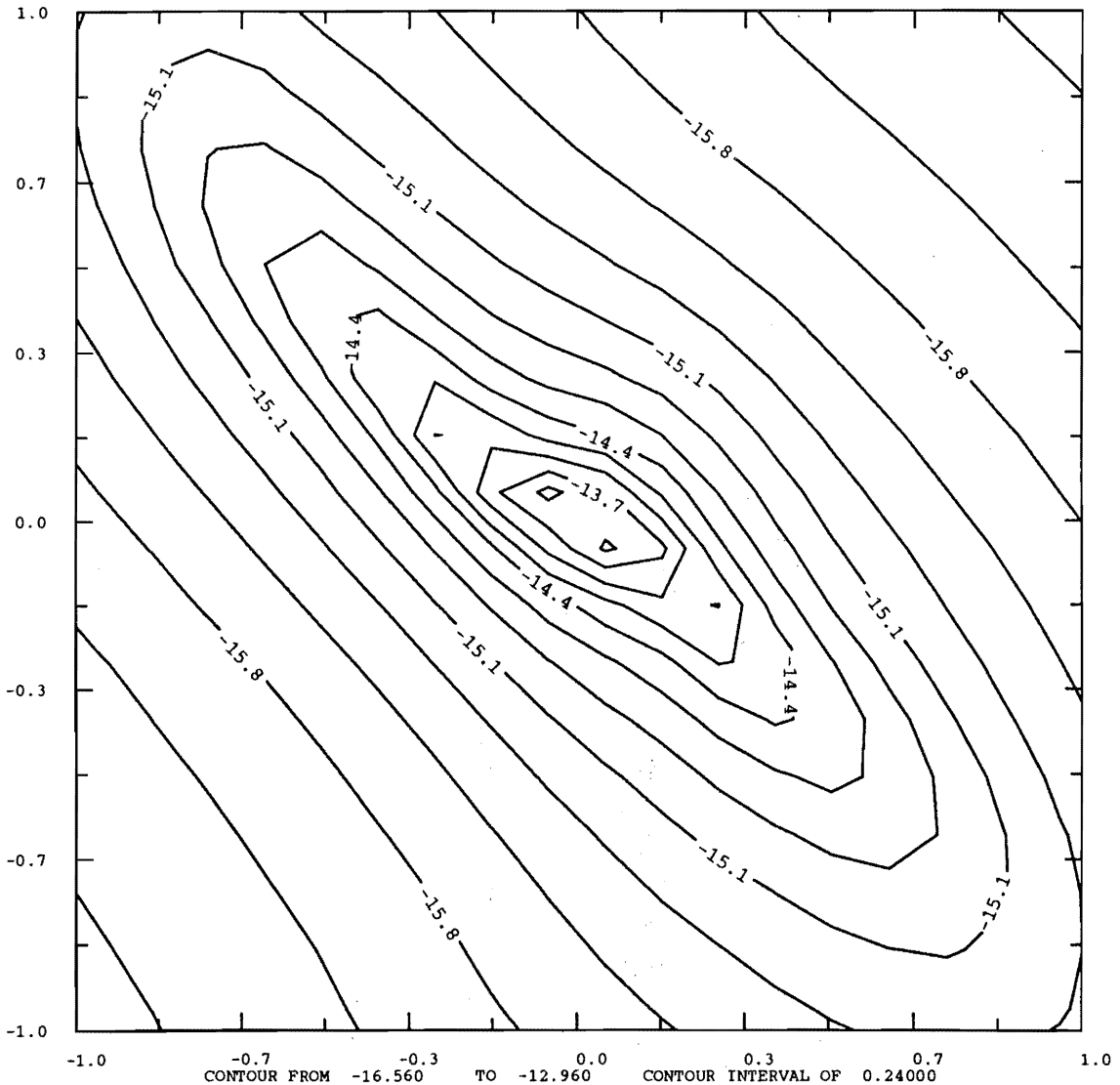
1.0
0.7
0.3
0.0
-0.3
-0.7
-1.0
-1.0
-0.7
-0.3
0.0
0.3
0.7
1.0
-15.1
-15.8
-14.4
-13.7
CONTOUR FROM -16.560 TO -12.960 CONTOUR INTERVAL OF 0.24000

FIG. 3d

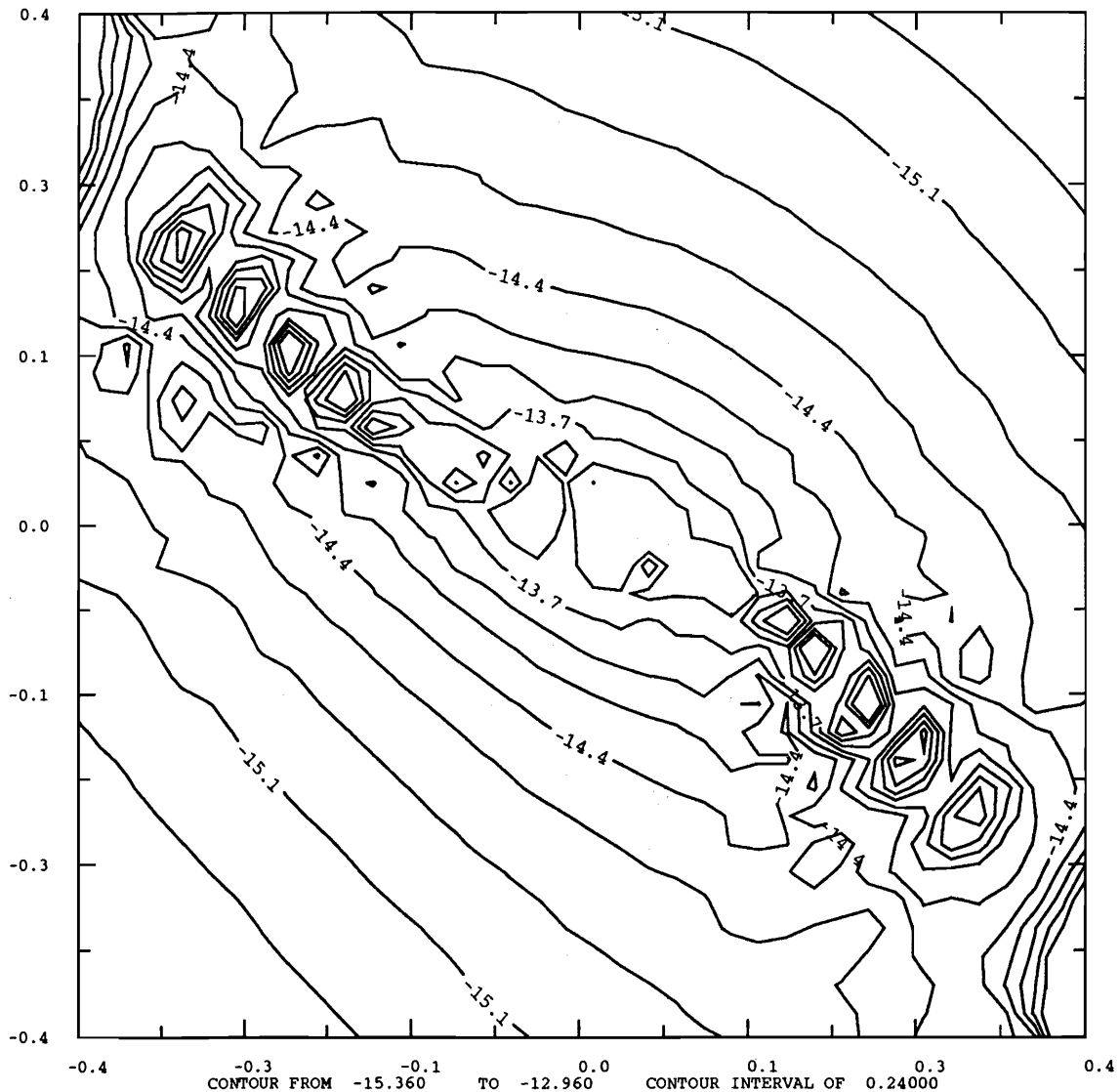
0.4
0.3
0.1
0.0
-0.1
-0.3
-0.4
-0.4
-0.3
-0.1
0.0
0.1
0.3
0.4
-15.1
-14.4
-13.7
CONTOUR FROM -15.360 TO -12.960 CONTOUR INTERVAL OF 0.24000

FIG. 4

(a)

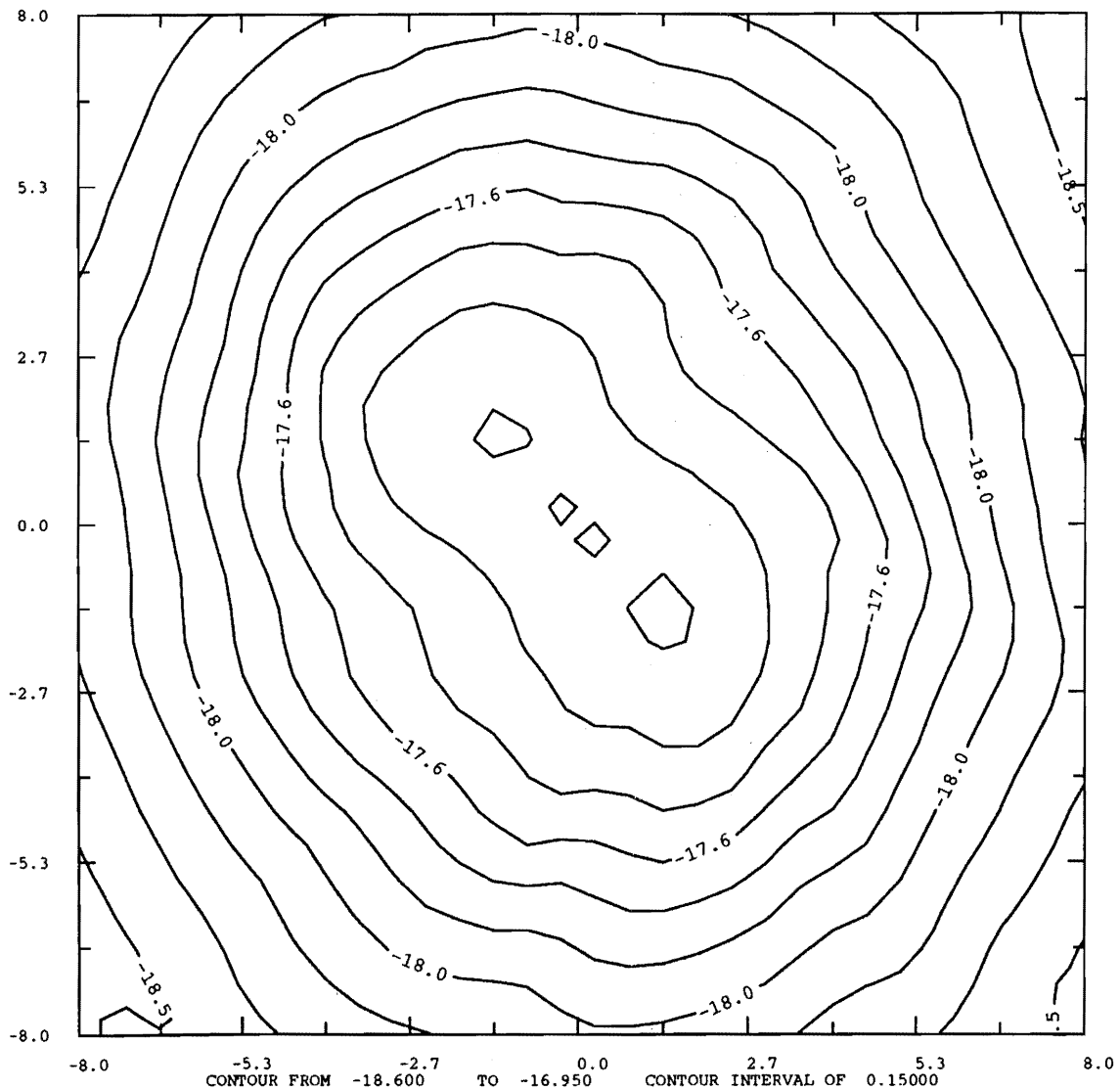
8.0
5.3
2.7
0.0
-2.7
-5.3
-8.0
-8.0
-5.3
-2.7
0.0
2.7
5.3
8.0
-18.0
-17.6
-18.5
CONTOUR FROM -18.600 TO -16.950 CONTOUR INTERVAL OF 0.15000

FIG. 5a

(b)

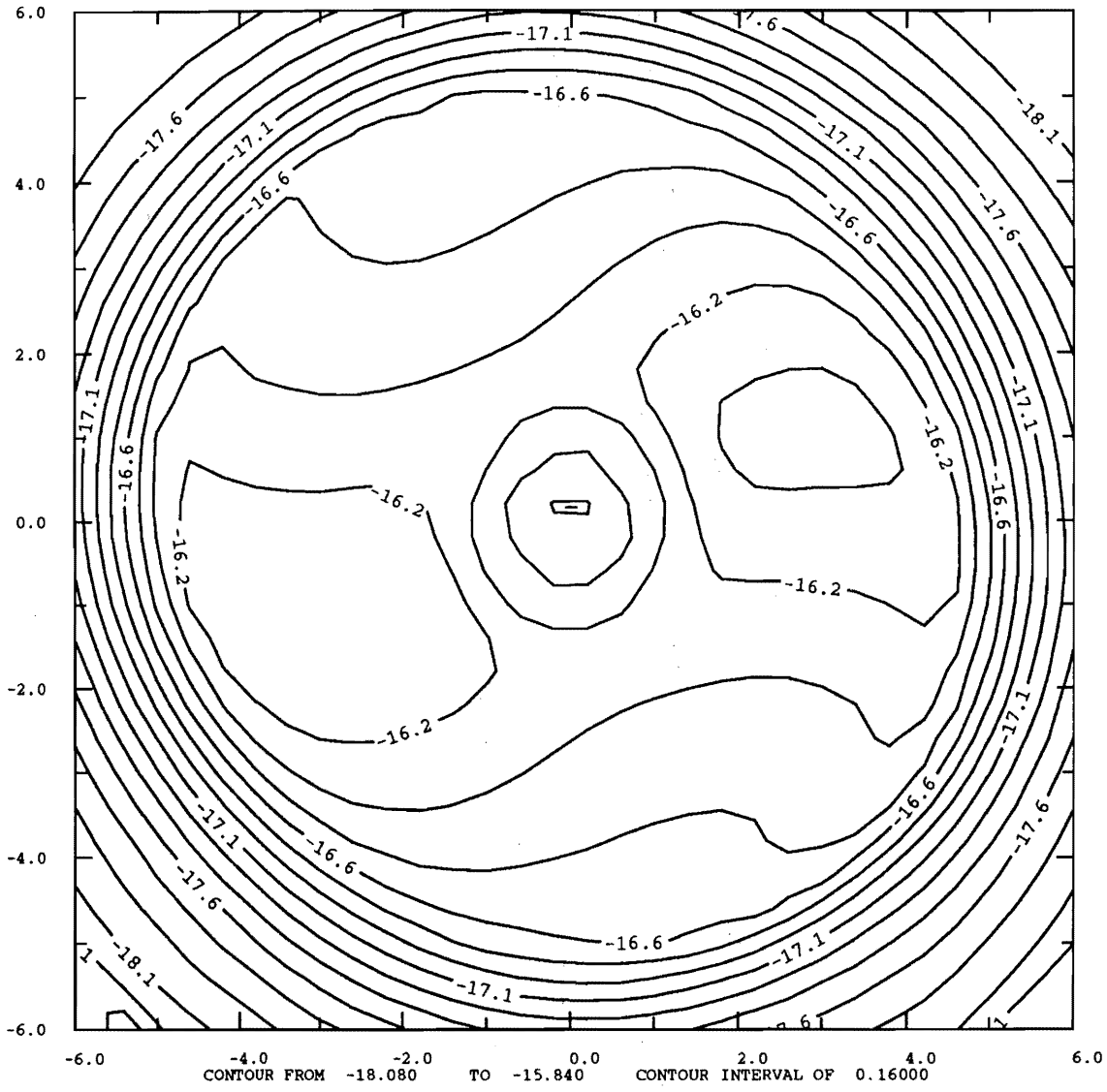
6.0
4.0
2.0
0.0
-2.0
-4.0
-6.0
-6.0
-4.0
-2.0
0.0
2.0
4.0
6.0
-17.1
-16.6
-17.6
-18.1
-16.2
CONTOUR FROM -18.080 TO -15.840 CONTOUR INTERVAL OF 0.16000

FIG. 5b

(c)

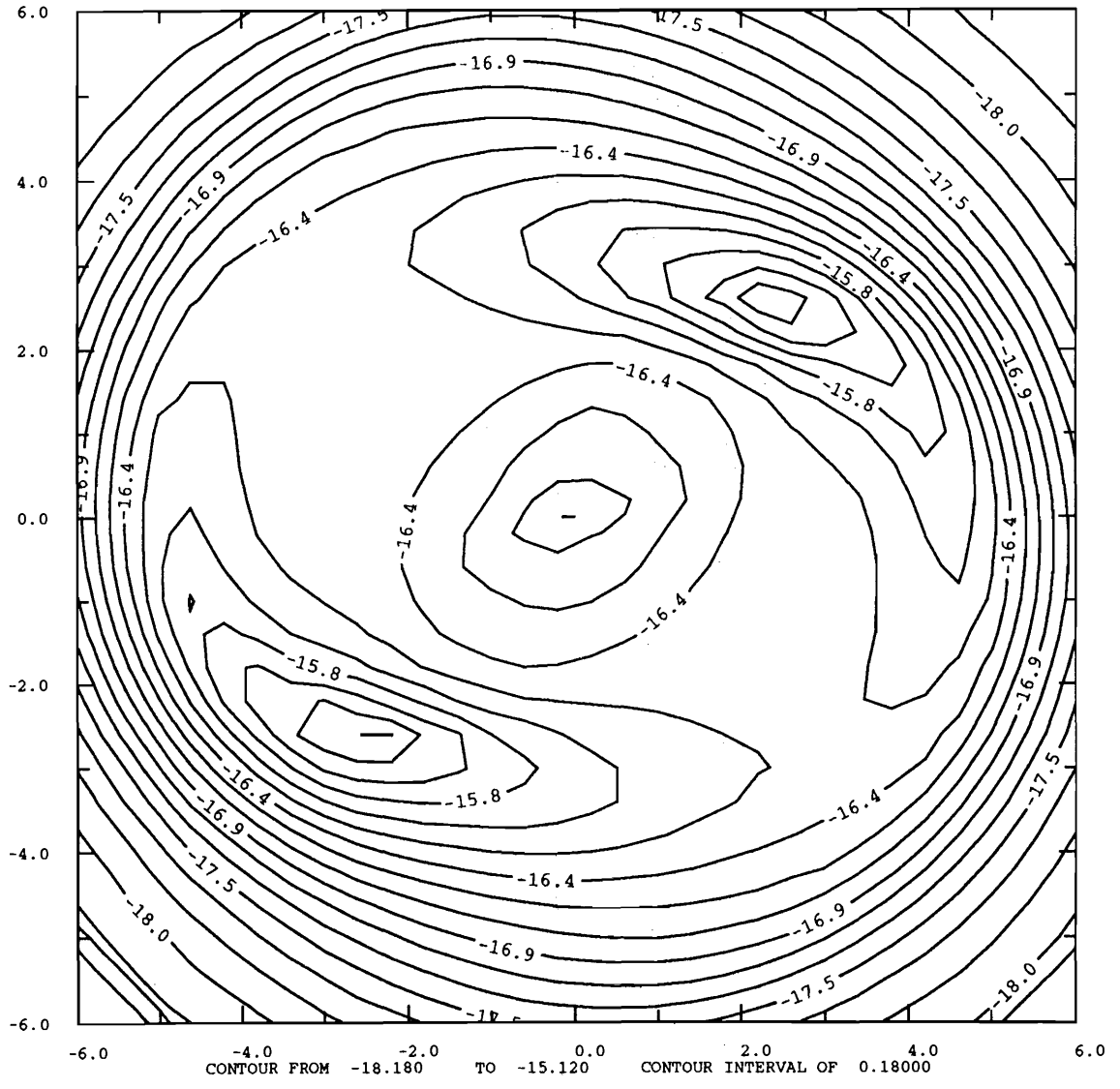
6.0
4.0
2.0
0.0
-2.0
-4.0
-6.0
-6.0
-4.0
-2.0
0.0
2.0
4.0
6.0
-17.5
-16.9
-16.4
-15.8
-18.0
CONTOUR FROM -18.180 TO -15.120 CONTOUR INTERVAL OF 0.18000

FIG. 5c

(d)

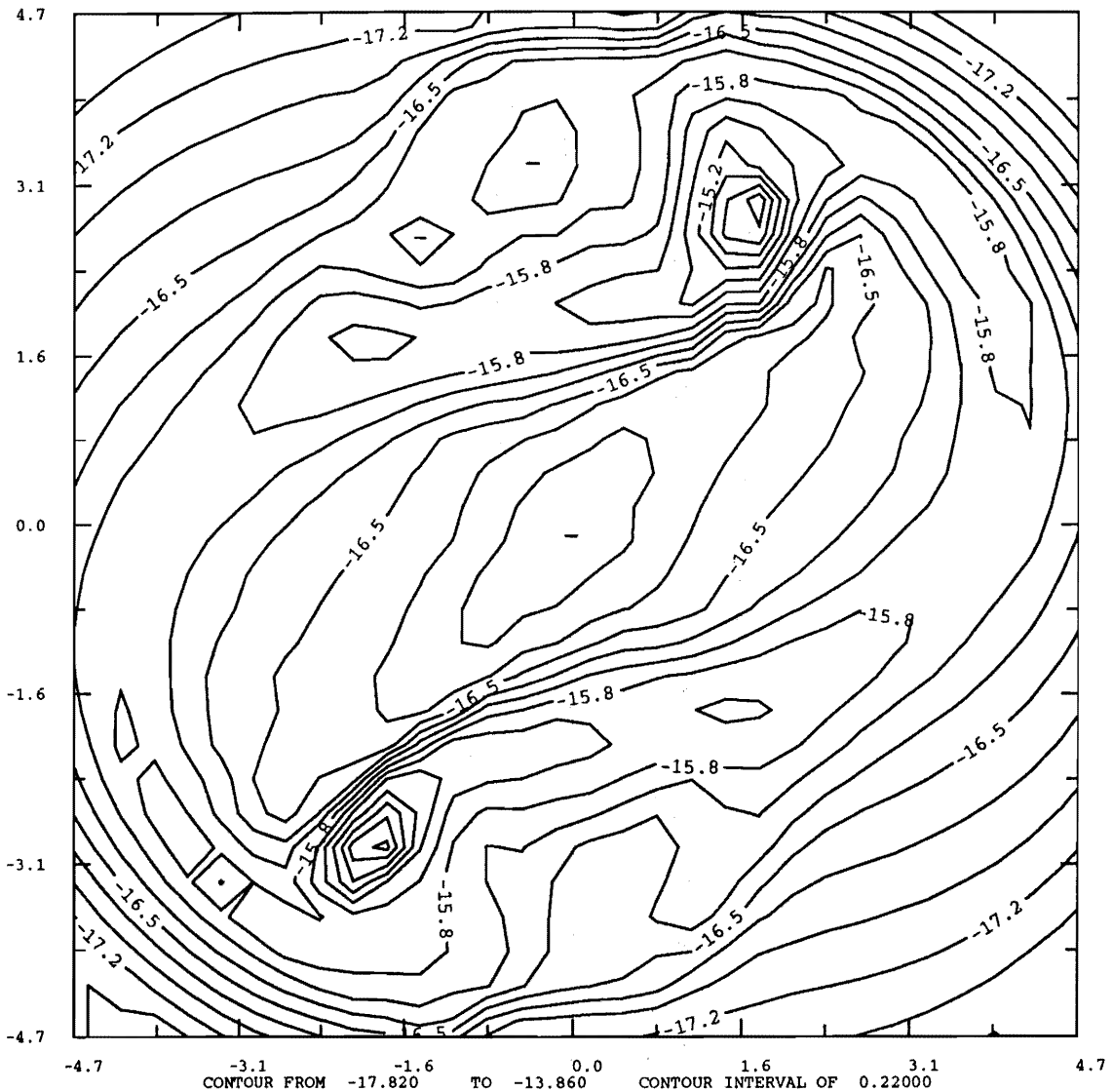
4.7
3.1
1.6
0.0
-1.6
-3.1
-4.7
-4.7
-3.1
-1.6
0.0
1.6
3.1
4.7
-17.2
-16.5
-15.8
-15.2
CONTOUR FROM -17.820 TO -13.860 CONTOUR INTERVAL OF 0.22000

FIG. 5d

(e)

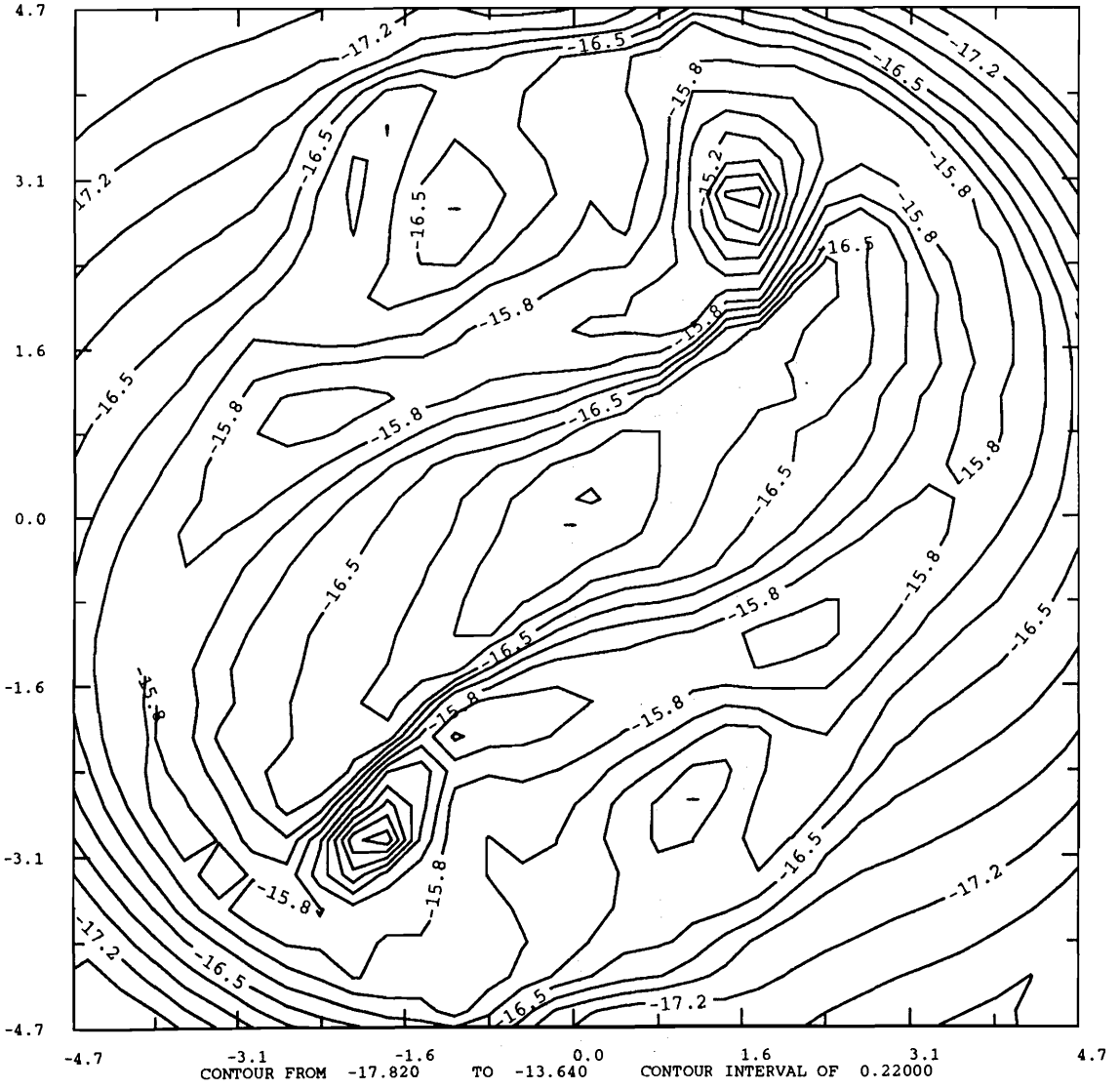
4.7
3.1
1.6
0.0
-1.6
-3.1
-4.7
-4.7
-3.1
-1.6
0.0
1.6
3.1
4.7
CONTOUR FROM -17.820 TO -13.640 CONTOUR INTERVAL OF 0.22000

FIG. 5e

(f)

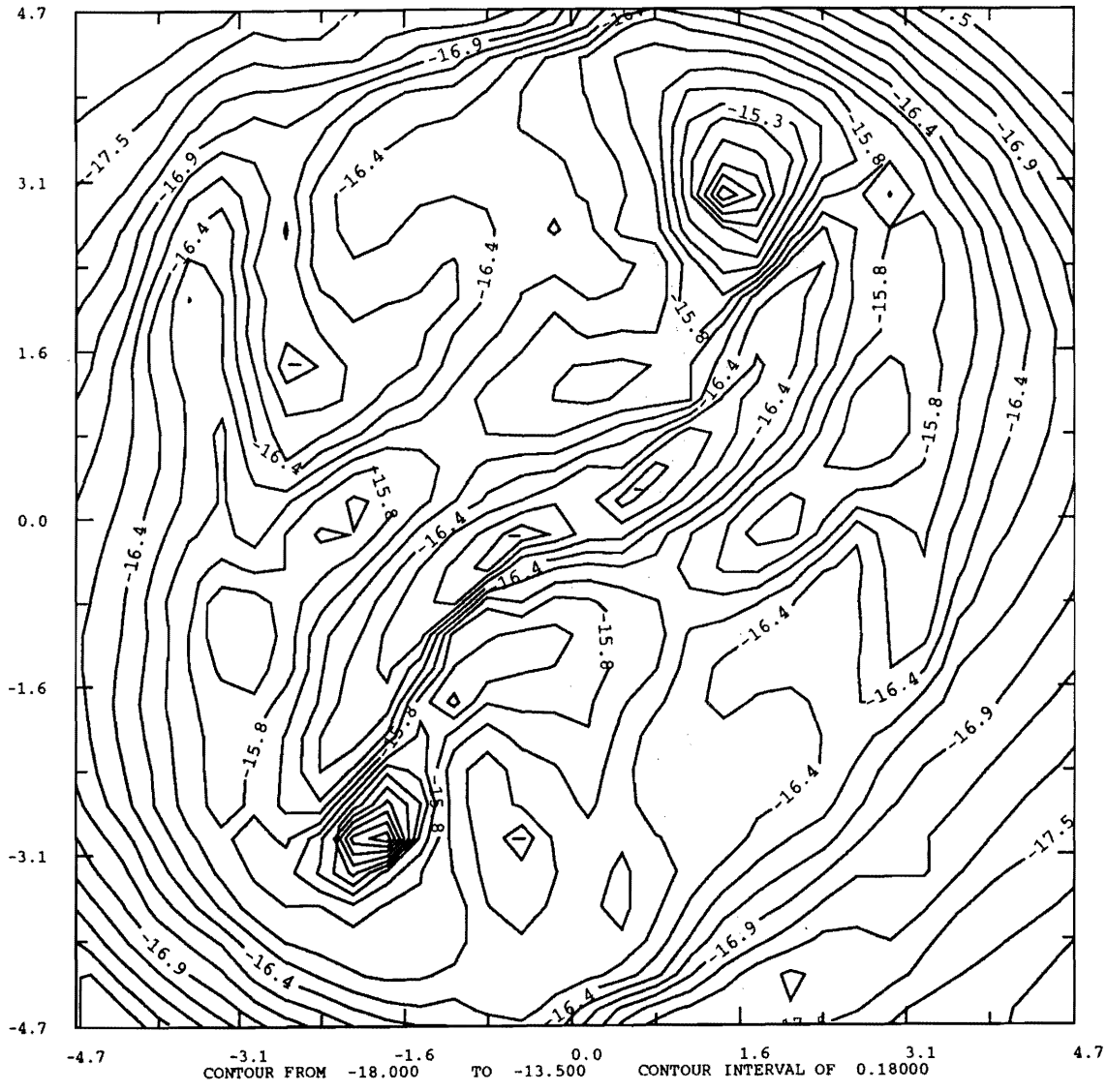
4.7
3.1
1.6
0.0
-1.6
-3.1
-4.7
-4.7
-3.1
-1.6
0.0
1.6
3.1
4.7
CONTOUR FROM -18.000 TO -13.500 CONTOUR INTERVAL OF 0.18000

FIG. 5f

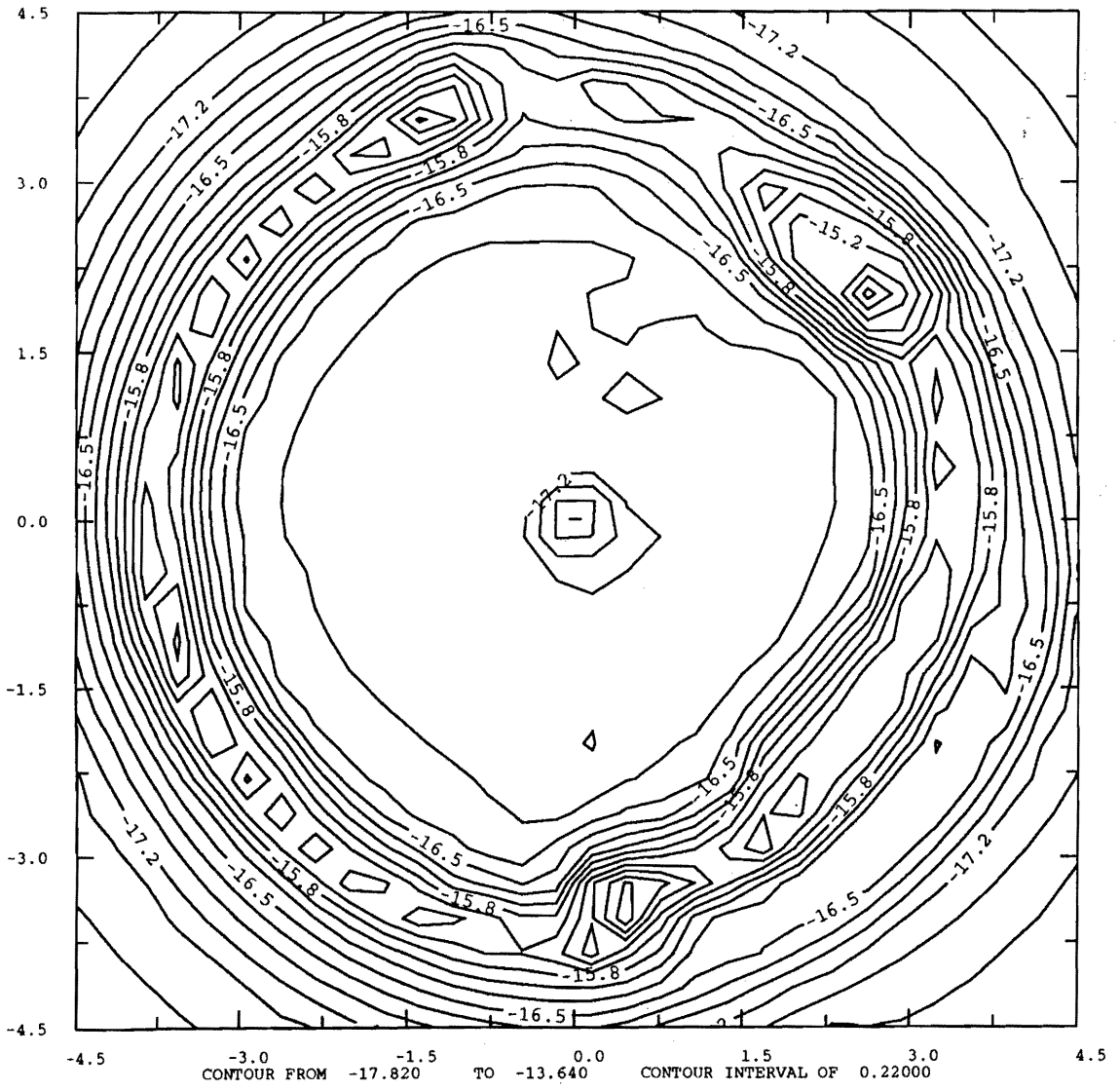
4.5
3.0
1.5
0.0
-1.5
-3.0
-4.5
-4.5
-3.0
-1.5
0.0
1.5
3.0
4.5
-16.5
-17.2
-15.8
-15.2
CONTOUR FROM -17.820 TO -13.640 CONTOUR INTERVAL OF 0.22000

FIG. 6